Boundary Lubrication and Surface Mobility of Mixed Alkylsilane Self-Assembled Monolayers

Qing Zhang and Lynden A. Archer*

School of Chemical & Biomolecular Engineering, Cornell University, Ithaca, New York 14853-5201

Received: June 5, 2003; In Final Form: September 5, 2003

We use a combination of experiment and theory to study the boundary lubrication characteristics of mixed self-assembled monolayers (SAMs) formed by tethering alkylsilanes with different chain lengths to planar substrates. The structure of mixed SAMs is characterized using atomic force microscopy, infrared spectroscopy, and hexadecane contact angle measurements. Lateral force microscopy is used to quantify the load and velocity dependence of friction force for one-component (pure) and two-component (mixed) SAMs. We find that if two-component SAMs and one-component SAMs are created with comparable packing density, the two-component systems possess lower friction coefficients. The friction force measured on silicon surfaces grafted with mixed SAMs increases linearly with the logarithm of sliding velocity over a broad range, whereas for pure SAMs, the friction force first increases linearly with the logarithm of velocity and then reaches a plateau. This plateau is believed to arise from the viscoelasticity of the tethered molecules. An analysis of the friction versus velocity data using a simple thermally activated Eyring model for a viscoelastic thin film shows that the lower friction coefficients of mixed SAMs are a consequence of higher mobilities of tethered molecules in the monolayer. This analysis yields characteristic relaxation times of 10^{-4} to 10^{-5} s for molecules in pure SAMs and relaxation times of 10^{-6} s in mixed SAMs. The estimated stress activation volume is in better accord with a surface flow mechanism where either a single molecule or possibly a subsection of a molecule participates in stress-activated motion during sliding contacts.

Introduction

Advances in silicon photolithographic process technology have led to the development of microelectromechanical systems (MEMS) over the last two decades. As the dimensions of these devices continue to decrease, control of surface interactions has quickly emerged as a key determinant of long-term mechanical durability.[1] A variety of surface modification techniques have been used to minimize friction and wear of MEMS devices.[2] The microscopic dimensions of the devices prohibit use of freely supported liquid lubricants that rely on viscous drag between multimolecular fluid layers to protect the moving surfaces. A preferred method of lubrication is to deposit dense coatings of organized, monomolecular liquid films to the substrates. Langmiur−Blodgett (LB) physical deposition and molecular self-assembly by chemical attachment of molecules to the surface are the two most common ways of creating these films.[2]

In the case of LB films, molecules interact with a substrate via weak van der Waals and ionic forces, and repeated shearing results in lubricant molecules being worn away.[3] Self-assembled molecules are covalently bonded to the substrates and are therefore not as prone to removal during multiple cycles of shear. The boundary lubrication properties of several different SAMs systems, including alkanethiols ($CH_3(CH_2)_{n-1}SH$) on Au, Ag, and Cu and alkyltrichlorosilanes ($CH_3(CH_2)_{n-1}SiCl_3$) on SiO_2 and mica, have been studied primarily by experiment.[4] Despite a large volume of work focusing on the effect of SAM order and chemistry on lubrication properties, very little is known about the fundamental relationships between friction coefficient of molecularly thin films and the mobility of molecules within the film.[5,6] Even less is known about the connection between SAM structure and molecular mobility.

The development of scanning probe microscopes (SPM), particularly atomic force microscopy (AFM), makes it possible to study interfacial phenomena on the molecular scale. This has led to many AFM or lateral force microscope (LFM) studies devoted to understanding the influence of thin film structure on friction properties.[7−9] Friction is observed to increase as the adhesive interactions between film surface and AFM tip increases, and significant variation of friction forces with molecular length was observed for several SAM systems.[3,10] The friction coefficient was found to decrease with increasing chain length and remains almost constant beyond a certain critical chain length (approximately 10 carbons). It was proposed that the poor packing of the shorter molecules results in more energy dissipation modes (chain bending and tilting, rotations, formation of gauche defects, etc), whereas these modes are sterically quenched in densely packed films formed by the longer chain molecules.

To further investigate the effect of film structure on its friction property and to gain more insight into the mechanism of boundary lubrication, it is important to study more complicated SAMs with nonuniform chemical compositions.[11] Several recent studies have focused on the frictional properties of two-component monolayers formed by coadsorption of molecules varying either in terminal group or in the length of the alkyl chain.[12−15] Friction studies using mixed alkanethiol SAMs, for example, showed that the conformational order and packing density profoundly influence their friction properties.[12,16] Mixed SAMs were found to be more liquid-like (more disordered) and to possess higher friction coefficients than pure SAMs. It was proposed that the greater disorder and higher concentration of gauche defects in mixed monolayers can raise their ability to dissipate energy during sliding.

10.1021/jp035592x CCC: $25.00 © 2003 American Chemical Society
Published on Web 11/01/2003

SAM systems based on alkylsilanes are better suited for lubricating crystalline silicon, polysilicon, or SiO_2 substrates used for fabricating MEMS. Alkylsilane SAMs have also been found to be more robust than the more widely studied alkanethiol SAMs due to their formation of a dense, cross-linked network of headgroups.[17] Stable mixtures of long and short alkylsilanes in a common solvent can self-assemble to form fully mixed (at least at a microscopic level) SAMs on silicate surfaces.[18] Although the boundary lubrication properties of these mixed SAM systems have received little attention, the composition and structure of the films can be controlled by varying the chain length and the compositions of the two adsorbates, allowing for in-depth understanding of the role of SAM structure on lubricant performance for MEMS.

In this paper, we present a systematic nanotribological study of alkylsilane mixed SAMs formed by varying the chain length and relative amounts of the two components. This approach minimizes the influence of variations in chemical composition and allows us to study the effect of thin film structure on boundary lubrication. The work also allows us to evaluate the general validity of the conclusions about friction properties of mixed SAMs reached on the basis of earlier work with alkanethiol systems. To relate film structure to boundary lubrication, we will use an Eyring-type model to capture the effect of SAM viscoelasticity on monolayer response in sliding contacts. The Eyring framework has been used in the past to describe molecular scale friction phenomena determined using the surface forces apparatus (SFA),[19] as well as from molecular dynamics simulations and lateral force microscopy measurements.[20,21]

Experimental Section

Preparation of SAMs. *n*-Butyltrichlorosilane (C4), *n*-decyltrichlorosilane (C10), *n*-hexadecyltrichlorosilane (C16), and octadecyltrichlorosilane (C18) were purchased from Gelest and used as received. Hexadecane ($C_{16}H_{34}$), chloroform ($CHCl_3$), methylene chloride (CH_2Cl_2), and ethanol (C_2H_5OH) were purchased from Aldrich chemicals. Three-inch polished silicon (100) wafers were obtained from University wafer and cut into 1 cm × 3 cm pieces using a diamond-topped stylus. These wafers were first cleaned with Kimwipes, rinsed with chloroform ultrasonically, and then treated with "piranha" solution (a mixture of concentrated H_2SO_4 and 30% H_2O_2 (7/3 (v/v)) at 100 °C for 30 min. ***Caution!*** **Piranha solution reacts violently with many organic compounds; use extreme care when handling it.** Clean substrates were rinsed thoroughly with deionized (DI) water and blown dry with a stream of nitrogen. The dry wafers were then transferred to a glovebox where they were stored in a dry nitrogen atmosphere.

Mixed monolayers were spontaneously formed by immersing clean silicon substrates into solutions of alkytrichlorosilanes dissovlved in 4:1 hexadecane/chloroform (10 mL total volume, 2 mM total alkyltrichlorosilane concentration). Standard solutions of alkyltrichlorosilanes were prepared in the glovebox filled with dry N_2 in glass volumetric flasks, and individual deposition solutions were prepared by transferring the correct amount of each standard silane solution to 25 mL glass vials, which had been cleaned by thoroughly rinsed with DI water and acetone and dried at 100 °C in an oven. After 24 h, the substrates were removed from the deposition solution and rinsed with 10 mL of CH_2Cl_2, $CHCl_3$, and ethanol to remove any residual organic contaminants. The monolayer was dried under a stream of nitrogen and then stored.

Contact Angle Measurements. Advancing contact angles of hexadecane on silicon substrates modified with mixed and pure SAMs were measured at room temperature and ambient relative humidity using a CAHN Dynamic Contact Angle Analyzer. Measurements using this method are sensitive to chemical changes within the first 5 Å of a material's surface. The force F_m generated when the substrate enters a test liquid, such as hexadecane, or when it just breaks free from the liquid, can be used to compute the surface tension γ_L of the liquid ($F_m = mg + p\gamma_L \cos(\theta) - F_b$). Here mg is the sample weight, $\gamma_L p \cos(\theta)$ ($\approx \gamma_L p$ at first and last contact) is the surface tension force acting on the meniscus (p is the wetted perimeter), and F_b is a buoyancy force. Once γ_L is determined from a first contact (advancing), or last contact (receding) experiment, the force measured when the probe translates slowly through the test liquid can be used to determine the equilibrium advancing contact angle (θ) of the liquid on the solid. Data were collected for at least three separate slides for each type of SAM and the results averaged.

Infrared Spectroscopy. Fourier transform infrared (FT-IR) transmission spectra of self-assembled monolayer films on silicon substrates were recorded using a Bruker Equinox 55 Fourier transform spectrometer at normal incidence. Spectra were collected over 500 scans at a spectral resolution of 4 cm^{-1}. A freshly cleaned silicon substrate was recorded before each series of measurements and used to determine the background spectrum.

AFM Measurements. A Dimension 3100 atomic force microscope (Digital Instruments) was used to characterize the surface topology and measure friction force. Experiments were performed in contact mode under ambient conditions of 20 °C and 40−50% relative humidity, and commercially available gold-coated V-shaped Si_3N_4 cantilevers with a announced force constant 0.12 N/m and tip radius 20−60 nm were used. Prior to an experiment, the tip was rinsed in methanol and dried in a laminar flow hood.

Surface friction force data were acquired by simultaneously scanning in the forward ($+x$) and reverse ($-x$) direction with disabled scanning in the y direction. An $+x/-x$ pair of scan lines provided a friction loop and its average width is a measure of the friction force. For friction coefficient measurement, the length of a scan was maintained at 1 μm and the scan rate at 2 Hz, giving a sliding velocity 4 μm/s. The applied load was varied by changing the vertical deflection of the cantilever, and each measurement reflects the average of at least five independent scans. For friction versus velocity measurements, the scan length was maintained at 0.5 μm for sliding velocities ranging from 0.1 to 2 μm/s, and at 10 μm for sliding velocities from 2 to 200 μm/s. After each velocity change, the friction force was allowed to reach its new steady state, generally after 5−10 scans, before friction data were recorded. To evaluate the effect of scan length on friction force, a second scanning procedure was used for sliding velocities in the range 0.5−50 μm/s. In this procedure the scan length was kept at 5 μm and the scan frequency was adjusted to achieve the targeted velocities. Comparison of the two sets of results indicates that, provided the scan length is maintained in the range 0.5−10 μm, friction force is independent of the scan length. The adhesion force between the AFM tip and the sample surface was measured via force−distance curves. Measurements were performed at several sites for each sample, and the average values were recorded. Before and after each friction measurement, AFM images of the sample surface were taken to ascertain the absence of damage.

To convert experimental normal (V_n) and lateral (V_l) deflection signals in voltage into normal (N) and lateral (f) forces in Newton, one has to obtain normal force calibration factor β

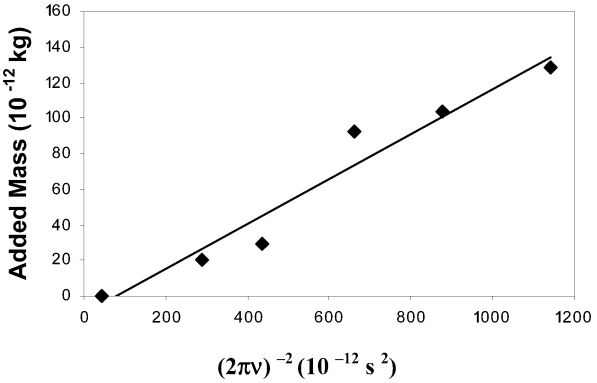

Figure 1. Added mass vs $(2\pi\nu)^{-2}$. Linear regression of the data gives a force constant of 0.127 N/m.

and lateral force calibration factor α, having unit of nN/V,[22]

$$N = \beta V_n = K_n S_n V_n \quad (1)$$

$$f = \alpha V_l = K_l S_l V_l \quad (2)$$

where K_n and K_l are normal and lateral force constants, and S_n and S_l are normal and lateral force optical deflection sensitivities. The normal sensitivity S_n can be readily obtained from the force−distance curve in AFM, and the lateral sensitivity S_l is related to S_n by a simple relation given by Evans.[23] The normal force constants K_n was determined by the added mass method proposed by Cleveland et al.[24] Briefly, the AFM tip was used as a micromanipulator to pick up a glass bead, and the new resonant frequencies were measured. A plot of added mass versus $(2\pi\nu)^{-2}$ (see Figure 1) yields a straight line with a slope equal to the force constant K_n. In this study, glass beads of diameters from 10 to 40 μm were used and the mass of a particle was calculated on the basis of the sphere radius measured by SEM and the bulk density of glass. The normal force constant of the cantilever was determined to be 0.127 N/m, which is close to the announced stiffness 0.12 N/m. When a series of experiments were completed, the cantilever/tip was then imaged using SEM to determine the dimension of the cantilever. The measured dimension parameters were then used to calculate the lateral force constant using an approach proposed by Noy et al.[25] The lateral force constant of the AFM tip used in the presented work is determined to be 223.6 N/m, and then the corresponding calibration factor α and β were obtained.

Results and Discussion

Characterization of the SAMs. The structure of one- and two-component SAMs was characterized by AFM, contact angle, and FT-IR measurements. Typical LFM images for pure and mixed SAMs are provided in Figure 2. The root-mean-squared roughness of C18 SAMs was determined by AFM topographic image analysis to be less than 0.3 nm, indicating complete and atomically flat films. Similar LFM images were observed for C10 and C16 pure SAMs, whereas the shorter chain (C4) monolayer is not as well formed. This observation is consistent with previous studies, which show that short chain molecules do not readily form well-ordered monolayer films by self-assembly.[3,10] It is believed that as the chain length increases to some critical value (∼10 carbons), the lateral cohesion between molecules can provide a crystalline structure and thus are more likely to form stable and robust coatings.

There has been much debate in the literature about the structure of mixed alkanethiol SAMs on gold. One school of thought is that phase separation occurs, leading to nanoscale domains populated with different adsorbates,[26,27] whereas for mixed alkyltrichlorosilane SAMs, kinetic studies by Offord et al. show that the alkyltrichlorosilanes adsorb with similar efficiency regardless of alkyl chain length and the shorter and longer chain molecules are therefore not expected to phase separate.[18] Fluorescence studies of mixed monolayers of alkyltrichlorosilane and (ω-vinylalkyl)- or [ω-(2-naphthyl)alkyl]-trichlorosilane prepared by coadsorption also show that the two components in the monolayers are fully mixed.[28] From Figure 2a,b, it can be seen that the film structure of pure C18 and mixed C4/C18 SAMs are similar. Parts c−f of Figure 2 also show no evidence of enhanced phase segregation in mixed SAMs down to length scales of order 80 nm, which indicates the two components are uniformly distributed (at least on the length scales resolved by AFM). It is nonetheless important to point out that for C4/C18 mixed SAMs, the packing density is comparable to the pure SAMs only for C18 compositions greater than about 0.5; at lower C18 compositions, poorly packed films were observed.

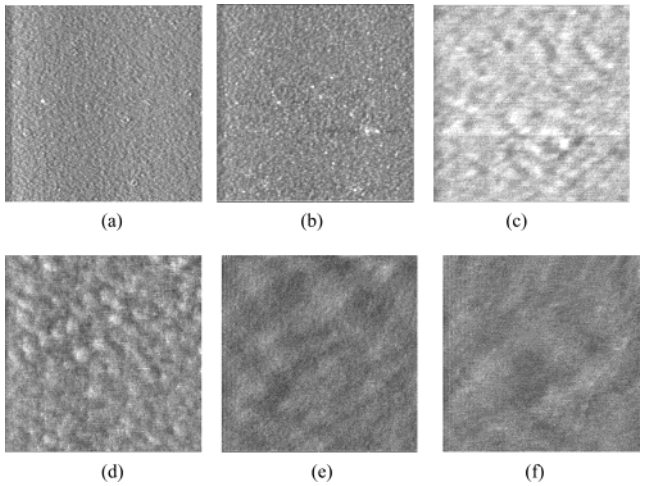

Figure 2. Lateral force images for pure and mixed alkylsilane SAMs on silicon: (a) octadecyltrichlorosilane (C18) monolayer, scan size 1 μm; (b) C4/C18 (1/1) mixed monolayer, scan size 1 μm; (c) C18, scan size 300 nm; (d) C4/C18 (1/1), scan size 300 nm; (e) C18, scan size 80 nm; (f) C4/C18 (1/1), scan size 80 nm.

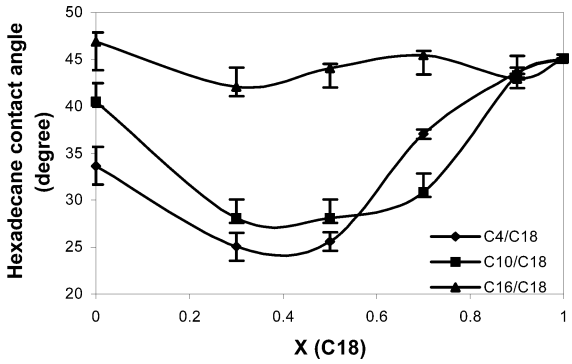

Figure 3. Variation of hexadecane advancing contact angle with composition of mixed C4/C18, C10/C18, and C16/C18 monolayers. *X* (C18) is the mole fraction of C18 in the deposition solutions of mixed SAMs. Recorded angles are averages of at least three measurements.

Figure 3 shows the advancing hexadecane contact angles plotted versus the composition of mixed C4/C18, C10/C18, and C16/C18 monolayers. For all three systems, nonmonotonic variations of hexadecane contact angle with composition are observed. The mixed SAMs are found to have lower contact angles than pure SAMs, and the minimum value is observed

when the ratio of the two components is nearly equal. The C4/C18 (ratio 1/1) mixed SAM has the lowest contact angle, and the C16/C18 mixed SAMs have contact angles similar to those of the pure SAMs over the whole range of compositions. Previous studies show that surface wetting of coatings by hexadecane is sensitive to the chemical makeup and structure of the material in the first 3 Å region near the surface.[29] This suggests that the interfaces of mixed SAM expose a mixture of CH_3 and CH_2 groups, the latter contributing to a higher energy surface, leading to a lower contact angle with hexadecane.[30] Furthermore, the increase of the effective contact area for mixed SAM due to surface disordering also leads to a lower contact angle. From the wetting data, it can be seen that as the fraction of the two components approaches 1/1 and as the chain length difference between the two components increases, the hexadecane contact angle will decrease, meaning the disordering of the surface region increases.

Transmission mode FT-IR spectra were obtained for all samples used in the study. We focus our attention on frequencies near the methylene symmetric $\nu_s(CH_2)$ and antisymmetric stretching modes $\nu_a(CH_2)$ (see Figure 4a). These peak positions are believed to be highly sensitive to the degree of order in SAM films.[31] Previous studies indicate that the peak position for $\nu_s(CH_2)$ and $\nu_a(CH_2)$ are typically in the range 2846−2850 and 2915−2918 cm^{-1} for all-trans extended chains and at ∼2856 and ∼2928 cm^{-1} for liquid-like disordered chains.[32,33] Figure 4b and c shows the peak positions of $\nu_s(CH_2)$ and $\nu_a(CH_2)$ plotted vs composition for the three systems. It is clear that the $-CH_2-$ stretching vibrations shift to higher frequency as the composition get closer to 1/1 and that the shift is larger for the mixed C4/C18 monolayers than for the C10/C18 and C16/C18 mixed SAMs at the same composition. These results are consistent with the contact angle data, confirming that the mixed SAMs possess more disordered structure than pure SAMs and that the disorder is largest when the difference in molecular weight is greatest and the ratio of the two components approaches 1/1.

The AFM, contact angle, and FT-IR data all indicate that pure SAMs composed of long alkysilane molecules (number of carbons > 10) have uniform, ordered structures composed of densely stacked molecules. For mixed SAMs of alkylsilanes with different chain lengths, the two components are thoroughly mixed, and the structure could be thought of as being a disordered hydrocarbon layer supported on a crystalline or liquid-crystalline underlayer. In this manner, the tail (the portion of the longer chains that extends beyond the end of the shorter chains) will contain gauche conformations with densities comparable to those in the liquid state, as indicated previously.[30]

Friction Measurements. Friction force versus applied load plots for several SAMs are presented in Figure 5a. The upper part of the $f-N$ curves can be approximated as a linear function, allowing the nominal friction coefficient μ for a particular SAM to be determined from the slope of a least-squares straight line fit to the data in the high load regime (20−80 nN). Values of μ obtained in this manner for all SAMs used in the study are summarized in Figure 5b. Due to scanning instabilities and data scattering in the negative and low load regime, it is difficult to tell from the experimental data whether the relationship between f and N in this load range is linear or sublinear.

It is evident from Figure 5b that the mixed SAMs have lower friction coefficients than pure SAMs and that the difference in friction coefficients between mixed and pure SAMs is substantial for the C4/C18 system but less obvious for the C16/C18 system. When Figure 5b is compared with wetting and FT-IR data, it is apparent that the friction coefficient decreases as disorder in the monolayer structure increases. This trend reverses in mixed SAMs with low packing density (e.g., C4/C18 with C18 compositions lower than 50%), where the friction coefficients of the mixed SAMs are found to be higher than that of the pure SAM composed of longer chains (C18). As discussed in the Introduction, previous studies with mixed alkanethiol SAMs suggest that mixed two-component monolayers always have higher friction coefficients than one-component monolayers.[12−15] This conclusion is clearly incorrect for alkyltrichlorosilane SAMs if the mixed and pure SAMs possess comparable packing density.

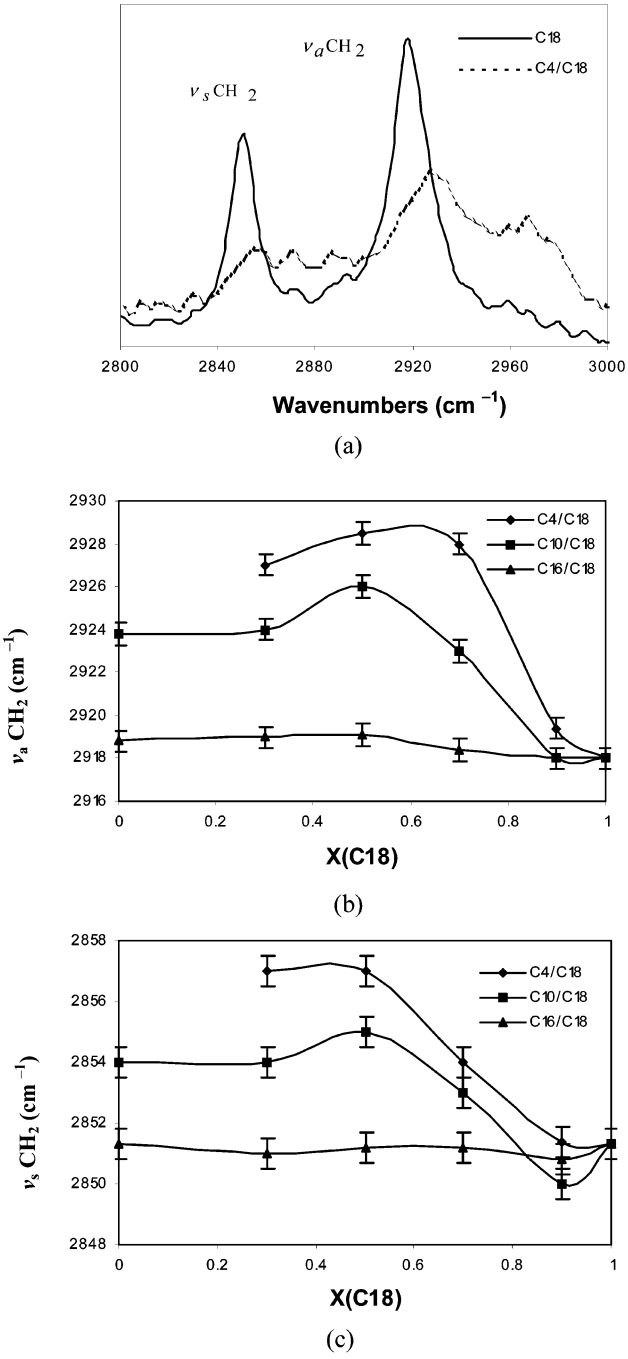

Figure 4. (a) Typical FT-IR transmission spectra (2800−3000 cm^{-1}) of pure (C18) and mixed (C4/C18: 1/1) alkyltrichlorosilane SAMs. (b) Antisymmetric methlyene band positions $\nu_a(CH_2)$ vs composition of monolayers. (c) Symmetric methlyene band positions $\nu_s(CH_2)$ vs composition of monolayers.

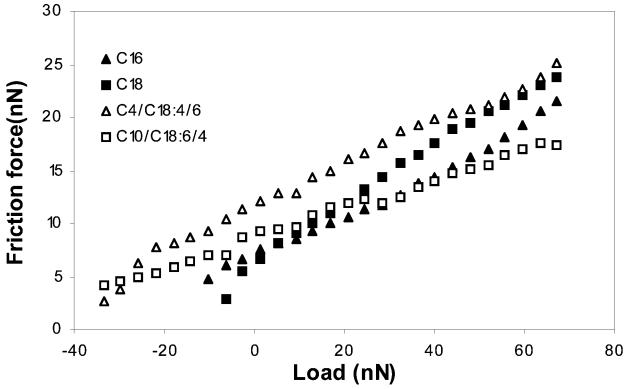

(a)

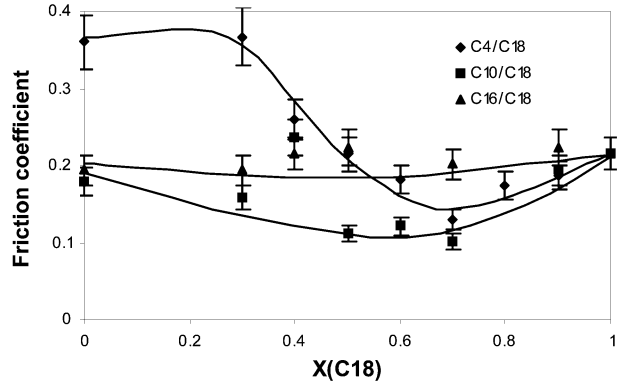

(b)

Figure 5. (a) Friction force vs applied load for some monolayers. (b) Variation of friction coefficient with composition of mixed SAMs. The same AFM tip was used for all the samples, and the sliding velocity was kept at 4 μm/s. The friction coefficient was determined from the slope of the least-squares fits of the $f-N$ curve in the load range from 20 to 80 nN.

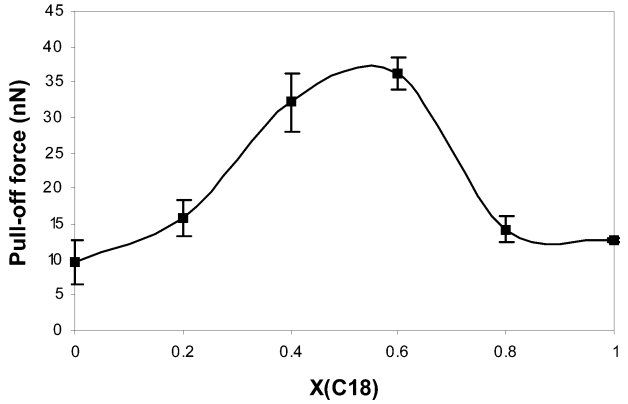

Figure 6. Pull-off force vs the composition for C4/C18 mixed SAMs.

The adhesion force (pull-off force) between the AFM tip and SAM surfaces was measured via the force−distance curve. Results for C4/C18 mixed SAM system are shown in Figure 6. It is observed that the mixed SAMs have higher pull-off forces compared with those of the pure SAMs. A similar result is observed for the C10/C18 system. Thus, contrary to popular belief, the decrease of friction force is not accompanied by a decrease of the pull-off force. Because the pull-off force is proportional to the Dupré energy of adhesion according to JKR theory,[34] the observed trends in adhesion forces suggest that the mixed SAMs have higher surface energies than pure SAMs, which is consistent with the contact angle data.

Additional insight into the relationship between monolayer film structure and surface friction properties can be obtained from the dynamic friction coefficient. For this purpose the friction force was measured as a function of sliding velocity for various one- and two-component SAMs. All measurements were performed at constant normal force N using the same AFM tip. Sliding velocities ranging from 0.1 to 200 μm/s are the primary focus of our study. The lower velocity limit is set by the instrument's noise threshold and the upper limit by the onset of wear. Friction force versus sliding velocity data for several SAMs are plotted in Figure 7. Each point is the average of at least two sets of independent experiments, and as discussed before, for scan lengths in the range 0.5−10 μm the friction force is independent of the scan length.

From Figure 7a,b, it can be seen that the dynamic friction behavior of mixed and pure SAMs are quite different. Figure 7a for example shows that at sliding velocities below 1 μm/s, SAMs are all characterized by similar $f-V$ curves. At higher velocities f becomes approximately proportional to log V over a range of velocities. For one-component C4 and C18 SAMs this velocity range is quite narrow and quickly transitions into a plateau. On the other hand, for the mixed SAMs, f versus log V is nearly linear for the entire range of velocities studied. Similar behavior is seen in Figure 7b for C10 pure and C10/C18 mixed SAMs. Figure 7c shows the $f-V$ curves for mixed (C16/C18) SAMs composed of alkylsilanes with similar chain length. In this case, little difference is seen between the $f-V$ curves for the pure and mixed monolayers and all show a transition to a plateau regime at $V \approx 10$ μm/s. Thus it appears that only monolayers with highly ordered surface structures (pure SAMs of higher molecular weight molecules (e.g., C16 and C18) and mixed SAMs such as C16/C18 composed of nearly identical components) manifest this transition in the experimental velocity range.

Theory. Additional insight into the relationship between SAM structure and friction properties requires fundamental understanding of how the molecular-scale determinants of friction (e.g., the surface mobility of tethered molecules in the monolayer) are affected by structure. Several phenomenological theories have been used previously for this same purpose.[35,36] Eyring-type models have been by far the most useful. The original mathematical model of activated processes was developed by Eyring[37] and later was adapted to describe the viscosity of liquids and plasticity of solids. It has been extended to interpret dissipation processes in macrosliding experiments by Briscoe and Evans[19] and has been used recently to interpret nanoscale boundary lubrication data on SAMs and LB films.[19−21]

The basic premise of Eyring's model is that the motion of a particular molecule in a material is restricted by potential barriers due to its neighbors. Relative motion between molecules is believed to occur when an applied stress or random thermal fluctuations provide sufficient energy to overcome the potential barrier.[37] Assuming a harmonic potential of barrier height Q, the average time t' for the molecule to pass across the barrier is the Boltzmann factor multiplied by the effective vibration frequency ν of the molecule:

$$\frac{1}{t'} = \nu \exp\left[-\frac{(Q + P\Omega - \tau\phi)}{kT}\right] \qquad (3)$$

where P is the pressure, τ is an imposed stress. The parameters Ω and ϕ are the so-called stress and pressure activation volumes, respectively. Briscoe and Evans showed that for a regular series of these barriers (see Figure 8) separated by a distance b, the average velocity v of the molecule (allowing

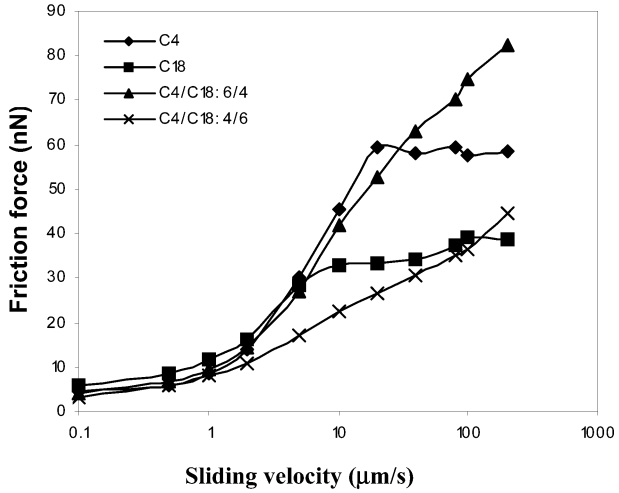

Figure 7. Friction forces as a function of sliding velocity for pure and mixed SAMs. All the samples were measured at a constant external load 47 nN using the same tip.

for transition in both directions) is given by

$$v = 2\nu b \exp\left[-\frac{(Q + P\Omega)}{kT}\right] \sinh\left(\frac{\tau\phi}{kT}\right) \tag{4}$$

The velocity v of the rate-controlling molecular process governing motion at a surface cannot be observed directly in a sliding friction experiment. Briscoe and Evans simply assumed that the sliding velocity V is proportional to v, $V = \alpha v$.[19] Introducing this assumption in eq 4 yields

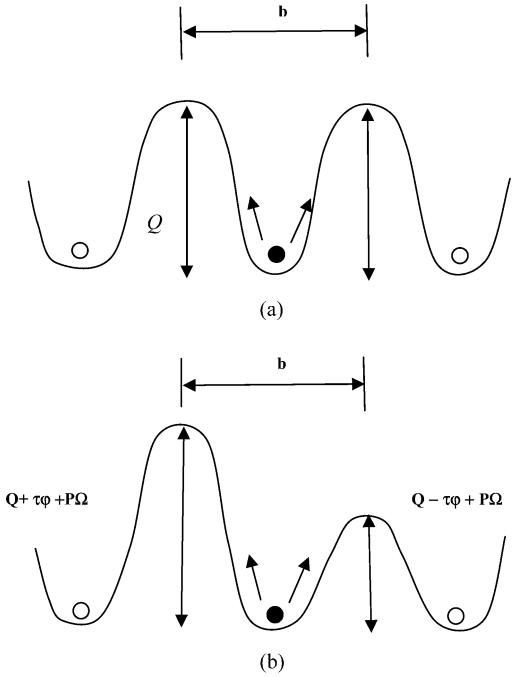

Figure 8. Double-well potential as described by the Eyring model: (a) no external stress; (b) under external shear stress and pressure.

$$V = 2V_0 \exp\left[-\frac{(Q + P\Omega)}{kT}\right] \sinh\left(\frac{\tau\phi}{kT}\right) \tag{5}$$

where $V = \alpha v$, and $V_0 = \alpha b \nu$.

In typical boundary lubrication measurements, $\tau\phi/kT > 1$, and eq 5 can be simplified to give

$$\tau = \frac{kT}{\phi} \ln(V/V_0) + \frac{(Q + P\Omega)}{\phi} \tag{6}$$

Thus, the sliding shear stress is predicted to increase with the logarithm of the sliding speed, and at fixed temperature, the stress activation volume can be determined from the slope of a plot of τ versus $\ln(V)$.

It is difficult to directly determine τ from micro- or nanofriction measurements because the contact area is not easily obtained. The friction force f is more easily obtained, so it is more useful to rewrite Briscoe and Evans' final result (eq 6) in terms of the friction force f. To begin, we assume the friction force is proportional to contact area A, whence

$$f = \tau A = \frac{AkT}{\phi} \ln(V/V_0) + \frac{A(Q + P\Omega)}{\phi} = \frac{A}{\phi}[kT \ln(V/V_0) + Q + P\Omega] \tag{7}$$

Considering the alternative case, $\tau\phi/kT \ll 1$. Taking the first term in Taylor series of $\sinh(\tau\phi/kT)$ in eq 5 yields

$$V \approx 2V_0 \exp\left[-\frac{(Q + P\Omega)}{kT}\right]\frac{\tau\phi}{kT} \tag{8}$$

Rearranging (8) gives

$$\tau = \frac{kT}{\phi}\exp\left[\frac{(Q + P\Omega)}{kT}\right]\frac{V}{2V_0} \quad (9)$$

$$f = \tau A = \frac{AkT}{\phi}\exp\left[\frac{(Q + P\Omega)}{kT}\right]\frac{V}{2V_0} = \frac{1}{2}EV \quad (10)$$

where

$$E = \frac{AkT}{V_0\phi}\exp\left[\frac{(Q + P\Omega)}{kT}\right]$$

Thus, we finally obtain the asymptotic forms of f for small and large friction forces,

$$f = \tau A = \frac{AkT}{\phi}\exp\left[\frac{(Q + P\Omega)}{kT}\right]\frac{V}{2V_0} \approx \frac{1}{2}EV \quad \text{for } \tau\varphi/kT \ll 1 \quad (11)$$

$$f = \frac{A}{\phi}[kT\ln(V/V_0) + Q + P\Omega] \approx B\ln V + D \quad \text{for } \tau\varphi/kT > 1 \quad (12)$$

where

$$B = \frac{AkT}{\phi} \qquad D = \frac{A(Q + P\Omega)}{\phi} - \frac{AkT}{\phi}\ln V_0$$

The contact area between the tip and surface obviously cannot be measured directly but can be estimated using contact mechanics.[34,38,39] According to JKR theory,[34,38] the contact area A as a function of applied normal force N on an AFM probe tip is given by

$$A = \pi\left(\frac{R}{K}\right)^{2/3}\{N + 3\pi R\gamma + [6\pi R\gamma N + (3\pi R\gamma)^2]^{1/2}\}^{2/3} \quad (13)$$

where R is tip radius, $\gamma = \gamma_1 + \gamma_2 - \gamma_{12}$, is the reduced surface tension and $K = {}^4/_3[(1 - \nu_1^2)/E_1 + (1 - \nu_2^2)/E_2]^{-1}$, is the reduced elastic Modulus.[34]

From eq 13 it can be seen that at constant normal force N, the factors that control contact area A are the reduced elastic modulus K and surface tension γ. According to JKR theory, the pull-off force F_a measured by AFM is directly related to the reduced surface tension γ by

$$F_a = -3\pi R\gamma/2 \quad (14)$$

As shown in Figure 6, the mixed SAMs have higher pull-off forces compared with those of pure SAMs, leading to higher values of γ. And for reduced elastic modulus, because the elastic modulus of the AFM tip (~300 GPa) is much larger than that of the monolayers (~1 GPa),[39,40] the reduced modulus will depend mainly on the SAM elastic modulus. Analysis of nanoindentation experiments on several monolayers using JKR theory shows that the elastic modulus of crystalline monolayers is higher than the modulus of liquid-like monolayers.[39] Therefore, we anticipate that at the same external normal force, the tip contact areas for mixed SAMs will be on average larger than those for the pure SAMs.

Comparison of Experimental Results with Theoretical Predictions. Friction force vs sliding velocity data for several SAMs is presented in Figure 7. As already pointed out, these results were obtained from atomic force microscopy using a single probe tip (nominal tip radius 50 nm) and at a fixed normal force. For one-component SAMs the friction force first increases with the logarithm of sliding velocity and then becomes nearly independent of velocity above a critical velocity value that changes from material to material. In the case of mixed SAMs a logarithmic relationship is evident over most of the velocity range studied. These observations are clearly in accord with expectations from eq 12, indicating that for the mixed SAMs $\tau\phi/kT > 1$ at nearly all sliding velocities. Introducing the normal force in eq 12 therefore yields

$$f = \frac{A}{\phi}[kT\ln(V/V_0) + Q + P\Omega] = \frac{AkT}{\phi}\ln(V/V_0) + \frac{AQ}{\phi} + \frac{N\Omega}{\phi} \quad (15)$$

From this equation, it is clear that the friction force at a fixed normal force depends mainly on A, ϕ, Q, and Ω.

Although it is possible that the plateau friction regime observed for the one-component SAMs may actually correspond to a broad maximum, our nanotribology measurements are limited by the onset of wear at higher velocities, making it impossible to determine the ultimate trend. In the work by Evans and co-workers on friction properties of LB films, a similar result was reported.[23,41] These authors observed quite different friction−velocity curves for different films. Though some monolayer systems manifested $f-V$ maximum at large sliding velocities, $f-V$ plateaus were observed for others. Li et al.[23] proposed that this difference is related to local phase transitions in the thin films induced by flow, but the precise origin of these phase transitions remains unclear.

Yoshizawa et al.[42] used the surface forces apparatus (SFA) to study friction of DHDAA monolayers on mica surfaces at various temperatures, sliding velocities, normal forces, and relative humidity. They found that with increasing temperature T the friction force first increased and then decreased. The authors speculated that the maximum in the $f-T$ diagram occurs when the time τ_l required for the monolayer surfaces to move laterally by some characteristic molecular length scale becomes comparable to the characteristic relaxation time τ_0 for molecular interdigitation of the alkyl chains. Under this condition the surface molecular groups have enough time to interdigitate as they pass each other but not enough time to completely disentangle, which leads to maximum energy dissipations. Yoshizawa et al. also argue that the friction force should exhibit similar behavior with sliding velocity.

Recently, Hadziioannou et al.[13] measured the friction force between unsymmetrical dialkyl sulfides molecules with varying chain lengths coated on planar gold surfaces and on AFM probe tips. The friction and adhesion force were measured as a function of load and sliding velocity. These authors reported that the friction force first increases linearly with the logarithm of sliding followed by a decrease after it reaches a maximum. The velocity at which the maximum friction occurs was found to be in the range from 1 to 10 μm/s, with the lowest values observed at the largest normal force. Hadziioannou et al. explained their findings using the same argument as Yoshizawa et al.[42]

Although the mechanism of chain entangling and disentangling proposed by Yoshizawa is plausible, it cannot be the process that causes the apparent plateau in the $f-V$ diagrams (Figure 7) for the one-component SAMs used in this work. Tupper[43] and Siepmann[44] showed that as a rigid AFM probe tip moves across a monolayer surface, it elastically compresses the chains ahead while pulling the chains behind the moving probe. Thus at least part of the work done by the lateral force on the tip, as it slides across the film surface, is consumed by compressing and stretching the surface-grafted chains. If the rate of compression and stretching exceeds the intrinsic relax-

ation rate of molecules in the monolayer, the viscoelasticity of the monolayer will influence the friction force measured.

This effect can be captured in the analysis presented earlier by reconsidering Briscoe and Evans' assumption that the molecular velocity v of the rate controlling process is simply proportional to the macroscopic sliding velocity V. Though this assumption is plausible at low sliding velocities (molecules have enough time to "keep-up" with the imposed cycles of compression and stretching), it becomes questionable when the sliding velocity is so large that the time required for molecules within the monolayer to move laterally by some characteristic molecular length scale becomes comparable to their longest relaxation time. Assuming that the characteristic molecular length scale for this process is δ and that the AFM probe tip slides at velocity V across the surface, the effective molecular velocity v can be written as

$$v = kVP(t) = kVP(\delta/V) \tag{16}$$

where k is a dimensionless constant and $P(t)$ is a time-dependent function that arises from the viscoelasticity of the monolayer. For surface molecules with a characteristic relaxation time τ_0, $P(t)$ can be written most simply as

$$P(t) = 1 - \exp(-t/\tau_0) \tag{17}$$

So, for t large in comparison to τ_0, $v = kV$ and the assumption that $V = \alpha v$ is good. On the other hand, when $\tau_0 \gg t$, $P(t) \approx t/\tau_0$ is time-dependent and the assumption is not good.

Substituting these results in eq 4, we find after some algebra,

$$f = \frac{A}{\phi}\left\{kT \ln\left[\frac{V}{V_0}\left(1 - \exp\left(-\frac{\delta}{V\tau_0}\right)\right)\right] + Q + P\Omega\right\} = B\ln\left[V\left(1 - \exp\left(-\frac{\omega_0}{V}\right)\right)\right] + D \tag{18}$$

where $\omega_0 = \delta/\tau_0$ and we have assumed $\tau\phi/kT > 1$ for simplicity.

Experimental data for one-component and two-component SAMs fitted to eq 18 are provided in Figure 9a. The corresponding best-fit parameters are listed in Table 1. It is apparent from the figure that eq 18 captures the experimental trends only in the velocity range of 1−200 μm/s. At lower velocities ($V <$ 1μm/s) the equation predicts a much too strong dependence of friction force on velocity and unphysical friction forces at the lowest velocities. These discrepancies are, however, not unexpected; they are, in fact, easily traced to the simplifying assumption $\tau\phi/kT > 1$ used in deriving eq 18. Considering the opposite limit, $\tau\phi/kT \ll 1$, we obtain from eq 11, $f \approx {}^1/_2 EV(1 - \exp(-\omega_0/V))$.

Combining the friction force for the two limiting cases gives

$$f = \frac{1}{2}EV\left(1 - \exp\left(-\frac{\omega_0}{V}\right)\right) \quad \text{as} \quad V < 1\ \mu\text{m/s} \tag{19}$$

$$f = B\ln\left[V\left(1 - \exp\left(-\frac{\omega_0}{V}\right)\right)\right] + D \quad \text{as} \quad V > 1\ \mu\text{m/s} \tag{20}$$

Using B and D from Table 1 to estimate E in eq 19 and combining the $f-V$ diagrams predicted by eqs 19 and 20 yields the results summarized in Figure 9b,c. In this case, eqs 19 and 20 capture the experimental trends for both one- and two-component SAMs over nearly the whole velocity range. The model parameters can be used to provide molecular-level information about the SAMs, which can be used to further elucidate connections between monolayer structure, relaxation dynamics, and boundary lubrication. For example, suppose the characteristic molecular length scale δ is of order 5 Å, then the characteristic relaxation time τ_0 of molecules in the SAMs can be determined from the parameter ω_0; the computed values are listed in Table 1.

From Table 1, it is apparent that the characteristic relaxation time for one-component SAMs is generally in the range 10^{-4} to 10^{-5} s and increases as the size of the tethered molecules

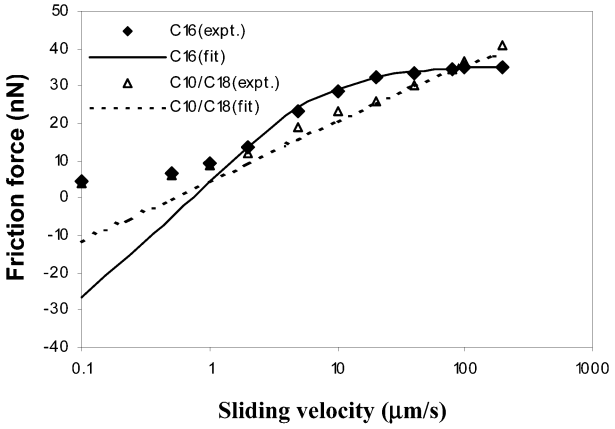

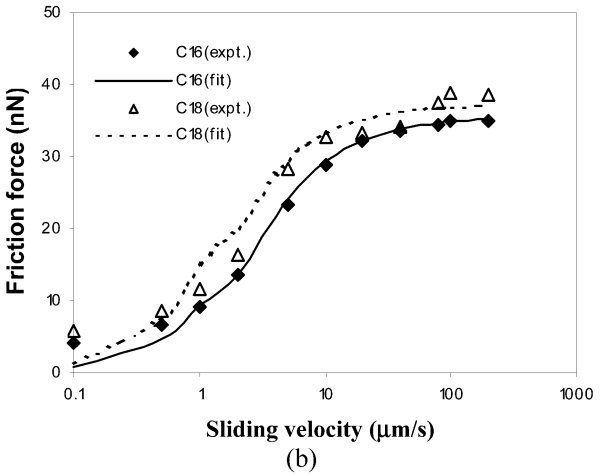

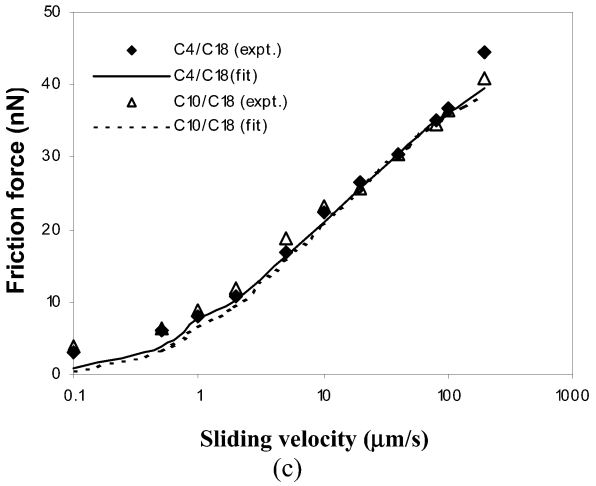

Figure 9. Fits versus experimental data for velocity dependence of friction force: (a) fits using eq 18; (b) and (c) fits using eqs 19 and 20. The compositions of mixed monolayers are Cn/C18: 1/1 (n = 4, 10, 16). The scattered symbols represent experimental data, and the solid or dashed lines represent the best-fit results. Similar levels of fitting are obtained for all the samples using the parameters in Table 1.

TABLE 1: Best-Fit Parameters for Pure and Mixed SAMs

compositions	B (nN)	D (nN)	ω_0 (μm/s)	τ_0 (10^{-5} s)
C4	25.1	−6.6	18	2.78
C10	14.4	0	11	4.55
C16	13.5	4.4	10	5.00
C18	17.4	9.5	5	10.00
C4/C18: 6/4	15.4	4.4	200	0.25
C4/C18: 4/6	6.7	5.6	300	0.17
C10/C18: 6/4	7.7	2.2	200	0.25
C10/C18: 4/6	7.2	4.4	200	0.25
C16/C18: 6/4	13.5	8.0	12	4.17
C16/C18: 4/6	16.4	0	12	4.17

increases. On the other hand, the characteristic relaxation time for two-component SAMs that manifest the lowest friction coefficients is, on average, at least 1 order of magnitude lower than that of the one-component systems. This result confirms our earlier finding that molecules in mixed SAMs are in a more disordered state. This finding is clearly important and can also be indirectly confirmed from the $f-V$ diagrams themselves. Specifically, if the onset of the high velocity plateau regime in the $f-V$ diagram coincides with the onset of viscoelastic behavior of the monolayer, as supposed in the analysis leading up to eqs 19 and 20, the absence of even the slightest hint of such a regime in the two-component SAM systems is consistent with their much lower characteristic molecular relaxation times. These characteristic times are nevertheless several orders of magnitude larger than relaxation times of molecular fluids. However, they are of the same order or lower than the characteristic relaxation times for monolayer films suggested by SFA and AFM studies based on the chain interdigitation mechanism.[13,42] These larger characteristic times for liquid monolayers clearly underscore the effect of surface confinement and ordering on molecular relaxation behavior in boundary lubricant films.

The parameter D is related to several unknown variables (Q, Ω, ϕ, and V_0) in the model. It is impossible to extract the value of any one of them from D. The parameter $B = AkT/\phi$, on the other hand, is simpler and therefore can provide insight into the fundamental length scale over which molecular processes dissipate energy during sliding contacts. Specifically, if the contact area A is known, it should be possible to estimate the stress activation volume ϕ from B. To estimate the contact area A using JKR theory or an extended Hertzian model, the tip radius R and Young's modulus E of the monolayer must be known. A wide range of E values (0.2−20 GPa) for monolayers can be found in the literature.[45−47] More careful indentation studies are required to determine which, if any of these values, characterize the SAM systems used in the present study. As a rough estimate, we compute ϕ values for the SAM systems from the respective B values for three different assumed E values, using the announced tip radius of 50 nm. These results are summarized in Table 2. Consider the case for the C18 one-component SAM, the estimated values of ϕ at the three different E values are 353.2 Å^3 (0.2 GPa), 115.2 Å^3 (1 GPa), and 27.7 Å^3 (9 GPa), respectively. It is apparent that irrespective of the E value chosen, these stress activation volumes are substantially lower than values determined by Briscoe and Evans ($\phi \sim 5$ nm^3).[19] Although it may be that the Young's modulus of C18 is even lower than 0.2 GPa, it is perhaps more likely that the difference arises from fundamental differences in the types of sliding contacts (multiasperity versus single point) used in the work by Briscoe and Evans and in the present study for measuring friction.

The exact physical meaning of the stress activation volume ϕ remains a matter of debate. Briscoe and Evans suggest that ϕ can be viewed roughly as a measure of the size of the molecular structure that moves during shear and Ω as the local increase in volume that accompanies shear.[19,20] In their study of alkanethiolate SAMs on gold, McDermott et al.[48] proposed that strong intermolecular interactions in ordered monolayers will hold a large block of molecules together during shear (increasing ϕ) and at the same time inhibit the formation of structural defects such as gauche kinks that would increase the volume change upon deformation (decreasing Ω). As a result, *n*-alkanethiolate monolayers formed from longer molecules, which have higher packing densities and more ordered structures, are thought to possess higher values of ϕ and lower values of Ω than shorter *n*-alkanethiolate monolayers.

TABLE 2: Stress Activation Volumes for Different Estimated Elastic Moduli[a]

	stress activation volume φ (Å^3)		
compositions	$E = 0.2$GPa	$E = 1$GPa	$E = 9$GPa
C4	244.5	79.7	19.1
C10	424.1	138.5	33.1
C16	454.4	147.9	35.7
C18	353.2	115.2	27.7
C4/C18: 6/4	397.4	129.3	31.2
C4/C18: 4/6	908.5	296.1	71.8
C10/C18: 6/4	795.2	259.3	62.6
C10/C18: 4/6	847.8	276.4	66.5
C16/C18: 6/4	454.0	147.9	35.8
C16/C18: 4/6	374.1	121.8	29.2

[a] Assuming the tip radius is 50 nm and the Poisson ratios for monolayer and tip are 0.3 and 0.5, respectively.

The volume per molecules for a pure alkysilane SAM can be estimated as $V_m = A_0L = 20 \times 25 = 500$ Å^3, where A_0 is the mean area per molecule on the monolayer surface and L is the thickness of the monolayer).[49] For one-component SAMs, this value is evidently comparable to ϕ at the lowest E values, whereas for mixed SAMs it is comparable to ϕ at intermediate E. One could alternatively estimate the characteristic molecular length scale ($\delta \approx \phi^{1/3}$), on which molecules move in response to the external shear stress during sliding contact. For all values of E, this length scale is in the range 2−10 Å, for the SAM systems used in the study. These values are consistent with the characteristic molecular length of 5 Å used in calculating the relaxation time. This is a strong indication that, for the SAM systems studied here, only a single molecule or a subsection of a molecule is involved in this energy dissipation process. Additional sliding friction studies using a wider range of alkylsilane and alkanethiol SAMs are underway in our group to help establish the generality of this last statement.

Conclusion

In this study, lateral force atomic force microscopy (AFM) measurements were used to study the friction of several one-component (pure) and two-component (mixed) alkylsilane self-assembled monolayers (SAMs). The mixed monolayer systems were created by simultaneous chemisorption of alkylsilanes with two discrete chain lengths. Surface packing density and crystalline order of the hydrocarbon tail groups of the SAMs were characterized by contact angle and Fourier transform infrared spectroscopy. These measurements indicate a systematic increase in surface disorder as the molecular weight of molecules is lowered in one-component systems and, in mixed SAMs, as the difference in molecular weight of the two components is varied and as the ratio of the components approaches 1/1. Structural variations induced in SAMs by molecular weight and blend composition were found to strongly influence their friction

properties. The magnitudes of the friction coefficient for mixed SAMs with high packing densities were found to be lower than the friction coefficients of one-component SAMs. This observation is opposite to previous findings for mixed SAMs formed from alkanethiols on gold, where mixed SAMs were always found to possess higher surface friction coefficients than one-component SAMs.

To understand the fundamental source of these observations, an Eyring-type model was developed to describe the dynamic friction properties of a viscoelastic surface film. This model predicts three distinct dynamic friction regimes. At low sliding speeds, the friction force is predicted to increase linearly with sliding velocity. At higher speeds, the friction force increases as the logarithm of velocity. Finally, at the highest speeds, the friction force becomes nearly independent of sliding speed. All three regimes were observed experimentally for one-component SAMs, but only the first and second regimes were seen for mixed SAMs. The absence of the third regime in the mixed SAMs was shown to be a direct consequence of the delayed onset of monolayer viscoelasticity, which can in turn be traced to a smaller value of the characteristic relaxation time of molecules in the two-component SAMs. Comparisons of the theoretical and experimental friction force−velocity diagrams indicate that the characteristic relaxation time for the one-component SAMs is in the range 10^{-4} to 10^{-5} s and of order 10^{-6} s for the two-component mixed SAMs. The estimated stress activation volume for both the mixed and pure SAMs ranges from a few tens to a few hundred cubic ångstroms and is consistent with the notion that only a single molecule, or possibly even a subsection of a molecule, is involved in stress-activated motion during sliding contacts between two rigid, nanosized substrates.

Acknowledgment. We are grateful to the National Science Foundation Tribology Program (Grant CMS0004525) and to the Department of Energy Nanosciences Program (Grant DE-FG02-02ER4600) for supporting this study. The AFM sliding friction measurements were performed using facilities of the Cornell Center for Materials Research (CCMR), a Materials Research Science and Engineering Center of the National Science Foundation (DMR-0079992).

References and Notes

(1) Bhushan, B. *Proc. Inst. Mech. Eng*. **2001**, Part J, 215.
(2) Lio, A.; Charych, D. H.; Salmeron, M. *J. Phys. Chem. B* **1997**, *101*, 3800.
(3) Maboudian, R.; Ashurst, W. R.; Carraro, C. *Sens. Actuators* **2000**, *82*, 219.
(4) Sung, M. M.; Kluth, G. J.; Yauw, O. W.; Maboudian, R., *Langmuir* **1997**, *13*, 6164.
(5) Heyes, D. M. *Tribol. Int.* **1996**, *29*, No. 8, 627.
(6) Liu, Y.; Wu, T.; Evans, D. F. *Langmuir* **1994**, *10*, 2241.
(7) Kaneko, R. *Tribol. Int.* **1995**, *28*, No. 3, 195.
(8) Bhushan, B. *Proc. Inst. Mech. Eng*. **1998**, Part J, 212.
(9) Hu, J.; Xiao, X.; Ogletree, D. F.; Salmeron M. *Surf. Sci.* **1995**, *327*, 358.
(10) Zhang, S. W.; Lan, H. Q. *Tribol. Int.* **2002**, *35*, 321.
(11) Tsukruk, V. V. *Adv. Mater*. **2001**, *13*, No. 2, 95.
(12) Shon, Y. S.; Lee, S.; Colorado, R.; Perry, S. S.; Lee, T. R. *J. Am. Chem. Soc*. **2000**, *122*, 7556.
(13) Van der Vegte, E. W.; Subbotin, A.; Hadziioannou, G. *Langmuir* **2000**, *16*, 3249.
(14) Beake, B. D.; Leggett, G. J. *Langmuir* **2000**, *16*, 735.
(15) Barrena, E.; Ocal, C.; Salmeron, M. *Surf. Sci.* **2001**, *482*−*485*, 1216.
(16) Perry, S. S.; Lee, S.; Shon, Y. S.; Colorando, R.; Lee, T. R. *Tribol. Lett.* **2001**, *10*, Nos. 1−2, 81.
(17) Kluth, G. J.; Sung, M. M.; Maboudian, R. *Langmuir* **1997**, *13*, 3775.
(18) Offord, D. A.; Griffin, J. H. *Langmuir* **1993**, *9*, 3015.
(19) Briscoe, B. J.; Evans, D. C. *Proc. R. Soc. London, Ser. A* **1982**, *380*, 389.
(20) Bouhacina, T.; Aime, J. P., Gauthier, S.; Michel, D. *Phys. Rev. B* **1997**, *56*, No. 12, 7694.
(21) Glosli, N.; McClelland, G. M. *Phys. Rev. Lett*. **1993**, *70*, 1960.
(22) Li, L. Y.; Yu, Q. M.; Jiang, S. Y. *J. Phys. Chem. B* **1999**, *103*, 8290.
(23) Liu, Y.; Evans, D. F. *Langmuir* **1996**, *12*, 1235.
(24) Clevland, J. P.; Manne, S.; Bocek, D.; Hansma, P. K. *Rev. Sci. Instrum*. **1993**, *64*, 403.
(25) Noy, A.; Frisbie, C. D.; Rozsnyai, L. F.; Wrighton, M. S.; Lieber, C. M. *J. Am. Chem. Soc*. **1995**, *117*, 7943.
(26) Tamada, K.; Hara, M.; Sasabe, H.; Knoll, W. *Langmuir* **1997**, *13*, 1558.
(27) Folkers, J. P.; Laibinis, P. E.; Whitesides, G. M. *J. Phys. Chem*. **1994**, *98*, 563.
(28) Mathauser, K.; Frank, C. W. *Langmuir* **1993**, *9*, 3002.
(29) Bain, C. D.; Whitesides, G. M. *J. Am. Chem. Soc*. **1988**, *110*, 5897.
(30) Laibinis, P. E.; Nuzzo, R. G.; Whitesides, G. M. *J. Phys. Chem*. **1992**, *96*, 5097.
(31) Allara, D. L.; Parikh, A. N.; Rondelez, F. *Langmuir* **1995**, *11*, 2357.
(32) MacPhail, R. A.; Strauss, H. L.; Snyder, R. G.; Elliger, C. A. *J. Phys. Chem*. **1982**, *88*, 334.
(33) Snyder, R. G.; Strauss, H. L.; Elliger, C. A. *J. Phys. Chem*. **1982**, *86*, 5154.
(34) Carpick, R. W.; Agrait, N.; Ogletree, D. F.; Salmeron, M. *Langmuir* **1996**, *12*, 3334.
(35) Yoshizawa, H.; Chen, Y. L.; Israelachvili, J. N. *J. Phys. Chem.* **1993**, *97*, 4128.
(36) Grosch, K. A. *Nature* **1963**, *197*, 858.
(37) Erying, H. *J. Chem. Phys.* **1935**, *3*, 107.
(38) Johnson, K. L. *Contact Mechanics*; University Press: Cambridge, U.K., 1987.
(39) Tsukruk, V. V.; Bliznyuk, V. N.; Hazel, J.; Visser, Dale. *Langmuir* **1996**, *12*, 4840.
(40) Ogletree, D. F.; Carpick, R. W.; Salmeron, M. *Rev. Sci. Instrum*. **1996**, *67* (9), 3298.
(41) Liu, Y.; Wu, T.; Evans, D. F. *Langmuir* **1994**, *10*, 2241.
(42) Yoshizawa, H.; Chen, Y. L.; Israelachvili, J. *J. Phys. Chem*. **1993**, *97*, 4128.
(43) Tupper, K. J.; Colton, R. J.; Brenner, D. W. *Langmuir* **1994**, *10*, 2041.
(44) Siepmann, J. I.; McDonald, I. R. *Phys. Rev. Lett*. **1993**, *70* (4), 453.
(45) Burns, A. R.; Houston, J. E.; Carpick, R. W.; Michalske, T. A. *Phys. Rev. Lett*. **1999**, *82*, 1181.
(46) Overney, R. M.; Meyer, E.; Frommer, J.; Guntherodt, H. J. *Lanmguir* **1994**, *10*, 1281.
(47) Chizhik, A. A.; Huang, Z.; Gorbunov, V. V.; Myshkin, N. K.; Tsukruk, V. V. *Langmuir* **1998**, *14*, 2606.
(48) Mcdermott, m. T.; Green, J. D.; Porter, M. D. *Langmuir* **1997**, *13*, 2504.
(49) Ulman, A. *Chem. Rev.* **1996**, *96*, 1533.